ChemPhysChem

Research Article
doi.org/10.1002/cphc.202400314

Chemistry Europe
European Chemical Societies Publishing

www.chemphyschem.org

Low-lying Negative Ion States Probed in Potassium – Ethanol Collisions

Ana Isabel Lozano,[a] Sarvesh Kumar,[a] Pedro J. S. Pereira,[a, b] Boutheïna Kerkeni,*[c, d] Gustavo García,[e] and Paulo Limão-Vieira*[a]

Dissociative electron transfer in collisions between neutral potassium atoms and neutral ethanol molecules yields mainly OH^-, followed by $C_2H_5O^-$, O^-, CH_3^- and CH_2^-. The dynamics of negative ions have been investigated by recording time-of-flight mass spectra in a wide range of collision energies from 17.5 to 350 eV in the lab frame, where the branching ratios show a relevant energy dependence for low/intermediate collision energies. The dominant fragmentation channel in the whole energy range investigated has been assigned to the hydroxyl anion in contrast to oxygen anion from dissociative electron attachment (DEA) experiments. This result shows the relevant role of the electron donor in the vicinity of the temporary negative ion formed allowing access to reactions which are not thermodynamically attained in DEA experiments. The electronic state spectroscopy of such negative ions, was obtained from potassium cation energy loss spectra in the forward scattering direction at 205 eV impact energy, showing a prevalent Feshbach resonance at 9.36 ± 0.10 eV with $\sigma^*_{OH}/\sigma^*_{CH}$ character, while a less pronounced σ^*_{OH} contribution assigned to a shape resonance has been obtained at 3.16 ± 0.10 eV. Quantum chemical calculations for the lowest-lying unoccupied molecular orbitals in the presence of a potassium atom have been performed to support the experimental findings.

1. Introduction

Ethanol (CH_3CH_2OH) and its isomer dimethyl ether (CH_3OCH_3) are relevant chemical compounds within the interstellar medium (ISM), although a general agreement has not been reached yet within the international community as to the formation routes of C_2H_5OH and CH_3OCH_3.[1,2] Apart from gas-phase reactions in different ISM environments that may lead to such molecules formation, e.g., in low-, intermediate- and high-mass star forming regions,[1,2] the proposed production routes may also involve interstellar cold grains, and so more complex surface induced reactions. For further details see Bergantini et al.[1] and Charnley and co-workers[2] (and references therein). Ethanol is also a relevant molecule within the Earth's atmosphere, with emission sources identified from natural, biogenic and anthropogenic origins, which may include natural plant fermentation processes, biomass burning and as a solvent in industrial/household applications, respectively.[3] From a global effort to reduce fossil fuels use,[4,5] and thus emission of greenhouse gases,[3,6] alcohol derivatives, including ethanol, have been considered as alternative chemical compounds acting as biofuels.[7–9]

Electron induced processes are prevalent in many different scientific and technological applications and a powerful mean to obtain spectroscopic information of key selected atomic and/or molecular targets. Therefore, studying the behaviour of electron interactions with ethanol is of pivotal relevance to understand the underlying molecular mechanisms responsible for anion formation and bond breaking. Low-energy electron interactions with ethanol result in negative fragment ions, with no evidence of parent anion formation.[10–16] This is in agreement with previous electron transfer experiments in high-energy (1–4 keV) collisions of H^-, O^-, and OH^- with C_2H_5OH molecules, albeit the differences observed in the anions' fragmentation pattern and their relative yields.[17] Dissociative electron attachment (DEA) experiments have been reported previously, while a general consensus on the nature of the accessible resonances has been reached. The lowest-lying shape

[a] Dr. A. I. Lozano, Dr. S. Kumar, Prof. Dr. P. J. S. Pereira, Prof. Dr. P. Limão-Vieira
Atomic and Molecular Collisions Laboratory, CEFITEC, Department of Physics, Universidade NOVA de Lisboa, 2829-516 Caparica, Portugal
and
Institut de Recherche en Astrophysique et Planétologie (IRAP), Université Toulouse III - Paul Sabatier, CNRS, CNES, 9 Avenue du Colonel Roche, 31028 Toulouse, France
and
Chemical Sciences Division, Lawrence Berkeley National Laboratory, One Cyclotron Road, Berkeley, 94720, California, USA
E-mail: plimaovieira@fct.unl.pt

[b] Prof. Dr. P. J. S. Pereira
Department of Mathematics, Instituto Superior de Engenharia de Lisboa, R. Conselheiro Emídio Navarro 1, 1959-007 Lisboa, Portugal

[c] Prof. Dr. B. Kerkeni
ISAMM, Université de la Manouba, La Manouba 2010 Tunisia
E-mail: boutheina.kerkeni@obspm.fr

[d] Prof. Dr. B. Kerkeni
Département de Physique, LPMC, Faculté des Sciences de Tunis, Université de Tunis el Manar, Tunis 2092, Tunisia

[e] Prof. Dr. G. García
Instituto de Física Fundamental, Consejo Superior de Investigaciones Científicas (CSIC), Serrano 113-bis, 28006 Madrid, Spain

Supporting information for this article is available on the WWW under https://doi.org/10.1002/cphc.202400314

resonance at ~2.8 eV has been assigned to a σ^*_{OH} antibonding molecular orbital, whereas those above 6 eV (6.35, 7.85 and 9.15 eV) to core-excited Feshbach resonances of $\sigma^*_{OH}/\sigma^*_{CH}$ characters.[10–12] The electronic state spectroscopy of neutral and negative ions has been probed by electron and photon interaction processes, the former include electron scattering,[18,19] electron impact spectroscopies[10,11,20–22] and theoretical methods on the vertical excitation energies of the neutral molecule,[19,22,23] whereas the latter on the lowest-lying neutral states by ultraviolet photoabsorption.[23–30] We also note C_2H_5O–H bond dissociation energies from experimental[31,32] and theoretical[31] methods, while electron driven dissociation from the core-excited Feshbach resonance at 6.35 eV,[10,11] is closely related to the parent Rydberg states in the high-resolution photoabsorption spectrum of Barbosa et al.[30] at 6.809 eV.

In this work, charge transfer time-of-flight mass spectra of anions formed in collisions between neutral potassium (K) atoms and neutral ethanol (C_2H_5OH) molecules have been investigated in the energy range from 17.5 to 350 eV in the laboratory frame (8.5 to 170.4 eV in the centre-of-mass frame). Additional relevant information has been obtained by recording a energy loss spectrum of potassium cations formed after the collision process in the forward scattering direction ($\theta \approx 0°$). Complementary information on the electronic structure of ethanol in presence of the potassium atom has been provided by *ab initio* quantum chemical calculations revealing the role of the most relevant lowest unoccupied molecular orbitals accessible in the electron transfer process. Electron transfer in neutral atom – neutral molecule collisions yielding ion-pair formation, is mediated by the crossing of covalent and ionic potential energy surfaces involving the atomic projectile and the molecular target, resulting therefore in fragmentation patterns that may differ from DEA processes.[33,34,43,44,35–42] For simplicity, let us take the case of a diatomic molecule (M), where the ionic potential energy curve lies above the covalent.[44] In the asymptotic limit, the endoergicity (ΔE) is given by $\Delta E = IE(K) - EA(M)$, with IE the ionisation energy of the potassium (K) atom and EA the electron affinity of the molecule. Upon electron transfer, $K + M \rightarrow (K^+ M^{-\#})$, and within the collision complex ($K^+ M^{-\#}$), the Coulomb interaction may prevail, thus delaying autodetachment long enough to allow intramolecular energy redistribution of the temporary negative ion (TNI) through the different available degrees of freedom. This may lead either to a stable parent anion or different fragmentation channels.

In the next section, we describe the experimental and theoretical methods, while section 3 is devoted to the results. Finally, conclusions from this work are summarized in section 4.

2. Experimental and Theoretical Methodologies

Time-of-flight (TOF) negative ion mass spectra as a function of the $K + C_2H_5OH$ collision energy, as well as K^+ energy loss measurements, have been obtained in a crossed molecular beam setup described elsewhere.[33,40,45] Briefly, a projectile beam of fast neutral K atoms crossed at right angles an effusive molecular beam target, and the product anions formed within the electron transfer process were analysed using a linear TOF mass spectrometer. The neutral K beam was produced in a resonant charge exchange chamber from the interaction of K^+ ions produced from a commercial ion source (HeatWave, US) in the energy range of 17.5 up to 350 eV in the laboratory frame (8.5 up to 170.4 eV in the centre-of-mass frame), with gas-phase neutral K atoms from an oven source. From the resonant charge-exchange process and the slits apertures, the potassium beam is mainly composed of potassium atoms in the ground-state configuration with its outermost electron as 4 s. This is supported by the experimental thresholds of formation which otherwise would result in values at lower energies (see Section 3) if K* in a 4p state were to be a relevant contribution. This is in accord with previous energy loss data from potassium collisions with pyrimidine,[33] halothane,[46] tetrachloromethane[45] and more recently with hexachlorobenzene[36,47] and water[48] probed in our laboratory.

The base pressure in the collision chamber was 5×10^{-5} Pa and upon ethanol admission the working pressure was 1×10^{-3} Pa. Anions formed in the collision region were extracted by a pulsed electrostatic field (340 Vcm^{-1}). The TOF anion yields were normalized to the primary beam current, pressure and acquisition time, and mass spectra ($m/\Delta m \approx 125$) were obtained by subtracting background measurements (without the sample) from the sample measurements. The TOF mass calibration was performed from the well-known fragmentation patterns from collisions of potassium atoms with CH_3NO_2 and/or CCl_4 molecules.[45,49]

Potassium cations formed post-collision were energy loss analysed in the forward scattering direction ($\theta \approx 0°$), while experiments were not performed in coincidence with TOF mass spectrometry. The analyser was operated in constant transmission mode, hence keeping the resolution constant throughout the entire scans. The estimated energy resolution during the experiments was ~1.2 ± 0.2 eV. The energy loss scale was calibrated using the K^+ beam profile from the potassium ion source serving as the *elastic* peak. C_2H_5OH was supplied by Sigma-Aldrich with a stated purity $\geq$ 99.8 % and was degassed through repeated freeze-pump-thaw cycles.

Finally, the different fragment anions thresholds in Figure 2 have been obtained from the TOF mass spectra, accounting for the ability to get a discernible signal at a given energy. From the energy resolution of the current experiments, we have scanned the collision energy of ± 0.5 eV from the expected energy for reactions (1)–(9) (see below).

2.1. Theoretical Method

Electronic structure investigations of the molecular orbitals (MOs) formed in collisions between potassium (K) atoms and ethanol (C_2H_5OH) have been performed to provide insight into the electron transfer process up to $\approx$12 eV. In particular, the analysis of the computed lowest unoccupied molecular orbitals is crucial to assess the nature of the different electronic states that result in the detected negative ions of the current experiments.

The geometry of ethanol + potassium system was initially optimised at the ωB97xD/gen level of theory and the equilibrium distance between the potassium K and oxygen O atoms is 2.73 Å. The ωB97XD is a range-separated version of Becke's 97 functional with additional dispersion correction is a good functional for determining excitation energies. The coordinates of the resulting optimised system can be seen in Figure 1. All quantum chemical investigations have been performed with the Gaussian 16 program package.[50] The calculations have been carried out in Cartesian coordinates, with no symmetries. All electrons have been taken into account for carbon, oxygen, hydrogen atoms with the aug-cc-pVTZ basis set, all potassium electrons have been treated through the valence triple ζ Def2TZVP basis set.[51,52] The combination of both basis sets is fairly flexible so the computed properties should be reliable to predict the desired electronic energies. The natural molecular orbitals for K-C_2H_5OH have been calculated by Density Functional Theory (DFT/ωB97xD/Gen) methods.[53] Within the negative ion, the excitation energies and oscillator strengths have been obtained at the TD-DFT level of theory up to 26 eV.

3. Results and Discussion

TOF mass spectra from electron transfer in potassium–ethanol collisions (17.5 to 350 eV in the lab frame, 8.5 to 170.4 eV in the centre-of-mass frame) yield fragment ions assigned to $CH_3CH_2O^-$, OH^-, O^-, CH_3^- and CH_2^-, with no evidence of parent anion formation; similar behaviour was also observed in methanol negative ion fragmentation upon electron transfer experiments.[54] Figure 2 shows the branching ratios (BRs) for the fragment anions of ethanol as a function of the centre-of-mass collision energy, while in Figure 3 we show the potassium cation (K^+) energy loss spectrum in the forward scattering direction ($\theta \approx 0°$) from K atoms in collisions with C_2H_5OH at 205 eV in the lab frame, 100 eV in the centre-of-mass frame, with assignment of the different features in Table 1.

The different TOF mass spectra recorded as a function of the collision energy, show the dominant ion assigned to hydroxyl anion followed by the dehydrogenated parent anion, the two contributing to more than 70% of the fragmentation yield. Interesting to note that $CH_3CH_2O^-$ yield only becomes close to OH^- at particularly high-collision energies (> 130 eV), albeit the EA(OH) ≈ EA(CH_3CH_2O) (see Table 2). In contrast DEA experiments show O^- as the main anion,[13] while other fragments than those listed here, e.g., CH_2CHO^-, HC_2O^- and H^- have been reported before.[10,14,15] Note that no discernible H^- signal from the background contribution was recorded for the collision energies probed, yet we do not discard the possibility of such anion being formed. In Figure 3 the energy loss spectrum peaks at $\Delta E = 13.7 \pm 0.1$ eV (I_{max}) which results in a vertical electron affinity of -9.36 ± 0.1 eV (EA(I_{max}) = IE(K)–ΔE, see Table 2 for IE(K)), in excellent agreement with the DEA Feshbach resonance at 9.15 eV.[10,13] The calculated lowest unoccupied molecular orbitals in the presence of a K atom in Fig. S1 show the main antibonding σ^*_{CO}, σ^*_{OH} and σ^*_{CH} characters along the C–OH, O–H and, C–H bonds, respectively.

Finally, at room temperature, one finds two conformers for ethanol, *trans* and *gauche* (+ and −) with C_S- and C_1-symmetry in their electronic ground states.[30] The electronic state spectroscopy of ethanol has been comprehensively investigated by high-resolution vacuum ultraviolet photoabsorption experiments and quantum chemical calculations, where the highest occupied molecular orbital (HOMO), 3a″/13a, is mainly due to O 2p lone pair orbital (n_O) perpendicular to the COH plane, whereas the second highest occupied molecular orbital (HOMO-1), 10a′/12a, has the O 2p orbital on the COH plane ($\bar{n}_O$) yet away from the direction of the C–O bond. For further details see Barbosa et al.[30] and references therein.

3.1. $CH_3CH_2O^-$ Formation

The dehydrogenated parent anion in electron transfer experiments can be formed via the following reaction:

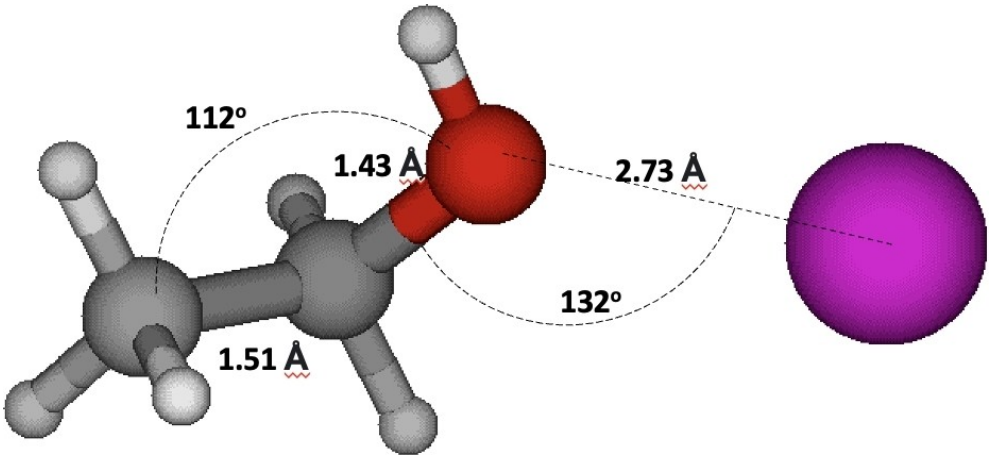

Figure 1. Molecular optimized structure of ethanol, and orientation of the K + C_2H_5OH collisional system. Colours are dark grey for C, red for O, light grey for H and magenta for K. Bond lengths are in Å, bond angles in (°).

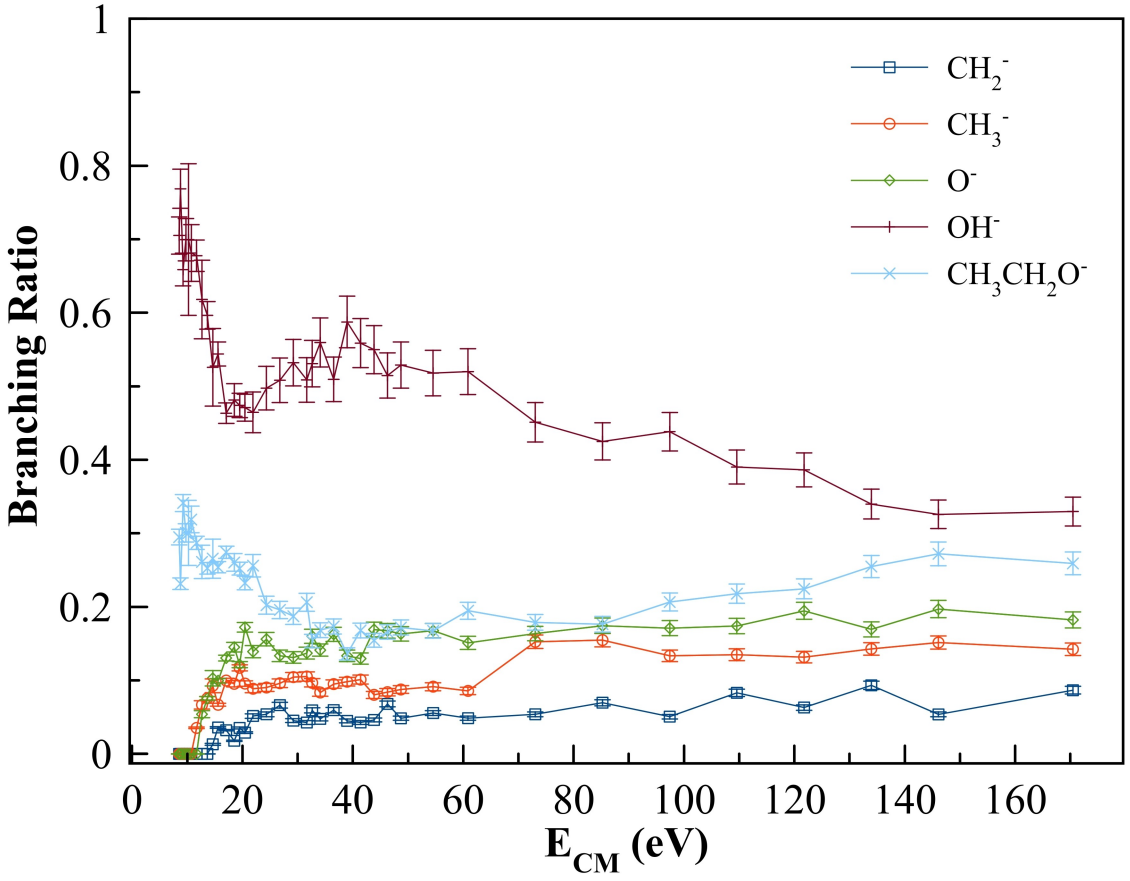

Figure 2. C_2H_5OH branching ratios (fragment anion yield/total anion yield) of the anions formed as a function of the collision energy in the centre-of-mass frame. Error bars are related to the experimental uncertainty associated with the ion yields. The solid lines were added just to guide the eye. See text for details.

Table 1. Assignment of different features from Gaussian fittings to K^+ energy loss spectrum from $K+C_2H_5OH$ collisions at 100 eV in the centre-of-mass frame. The uncertainties result from the Gaussian fitting procedure (values in eV).

K^+ Energy Loss Feature	Vertical Electron Affinity	Calculated vertical energy of MOs		Assignment[a]	DEA resonances
		neutral	negative ion		
7.5 ± 0.1	−3.16 ± 0.10	3.13	2.25	σ^*_{OH}	2.88[12]/~2.0[13] ($CH_3CH_2O^-$)
10.9 ± 0.2	−6.56 ± 0.20	6.20	6.23	$\sigma^*_{OH}/\sigma^*_{CH}$	6.35[12]/5.8[13] ($CH_3CH_2O^-$); 5.5[13] (O^-); 6.4[14] (H^-)
12.3 ± 0.1	−7.96 ± 0.10	7.99/8.65	8.22	$\sigma^*_{OH}/\sigma^*_{CH}$	7.85[12] /~8.0[13] ($CH_3CH_2O^-$); 8.2[13] (OH^-); 7.8[14] (H^-)
13.7 ± 0.1	−9.36 ± 0.10	9.37/9.59	9.36	$\sigma^*_{OH}/\sigma^*_{CH}$	9.15[12] ($CH_3CH_2O^-$, OH^-); 9.3[14] (H^-)
15.5 ± 0.1	−11.16 ± 0.10	11.16/ 11.23	11.29	[b], $\sigma^*_{CC}/\sigma^*_{CO}/\sigma^*_{CH}$	–
17.4 ± 0.1	−13.06 ± 0.10	–	13.16	[c]	–
19.0 ± 0.1	−14.66 ± 0.10	–	14.50	[d]	–
20.4 ± 0.1	−16.06 ± 0.10	–	16.42	[e]	–
22.2 ± 0.2	−17.86 ± 0.20	–	17.54/18.18	–	–
24.1 ± 0.4	−19.76 ± 0.40	–	19.78	–	–
26.6 ± 0.3	−22.26 ± 0.30	–	22.48	–	–
30.0 ± 0.3	−25.66 ± 0.30	–	25.89	–	–

[a] see Figs. 3 and S1; [b] $\bar{n}_O/\sigma_{CO}\rightarrow(n+1)/(n+2)d$; $\sigma_{CC}\rightarrow(n+1)/(n+2)p$; $n_O/\sigma_{CC}\rightarrow(n+1)/(n+2)p$; $\bar{n}_O/\sigma_{CC}\rightarrow(n+1)/(n+2)d$; [c] $\sigma_{CO}\rightarrow(n+1)/(n+2)p$; $\sigma_{CC}\rightarrow(n+1)/(n+2)p$; $\bar{n}_O/\sigma_{CC}\rightarrow(n+1)/(n+2)p$; $n_O/\sigma_{CC}\rightarrow(n+1)/(n+2)d$; [d] $\bar{n}_O/\sigma_{CC}\rightarrow(n+1)/(n+2)p$; $n_O/\sigma_{CC}\rightarrow(n+1)/(n+2)p$; [e] $n_O/\sigma_{CC}\rightarrow(n+1)/(n+2)p$;

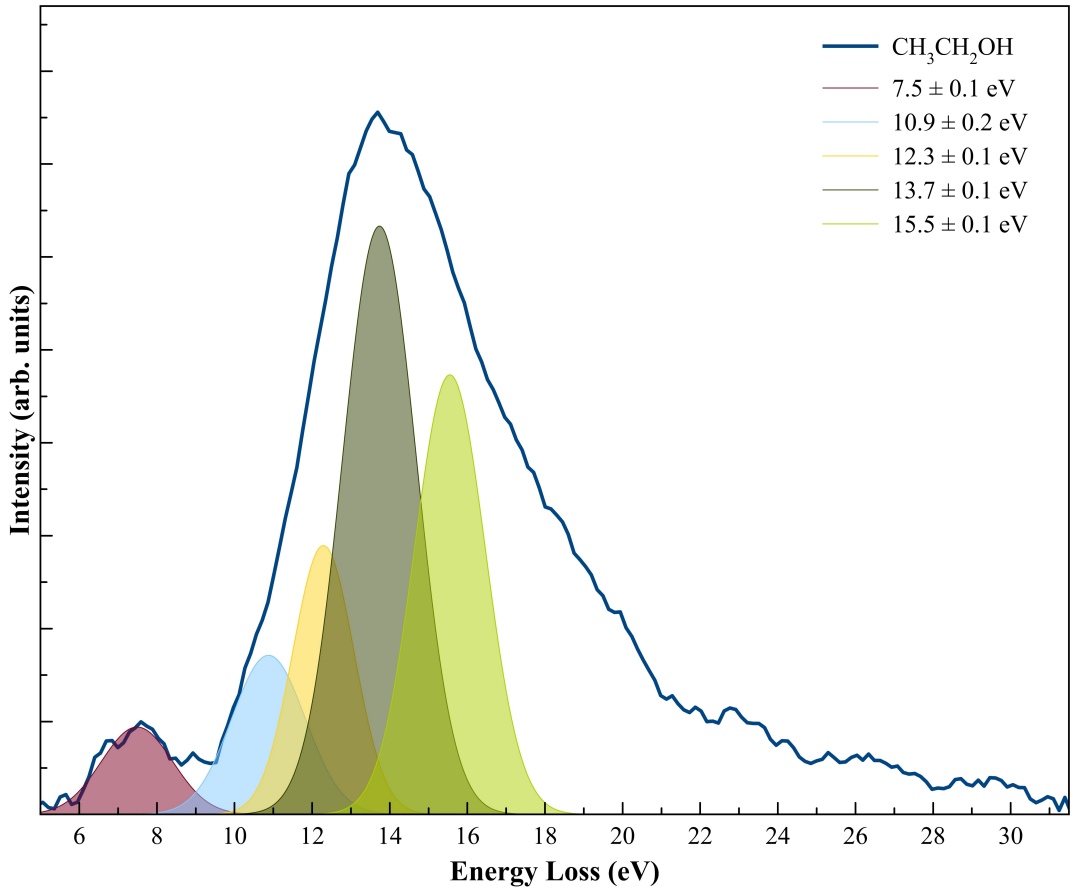

Figure 3. Energy loss spectra of K^+ in the forward scattering direction ($\theta \approx 0°$) at an impact energy of 100 eV in the centre-of-mass frame for $K + C_2H_5OH$. The peaks' maxima are related to the estimated vertical excitation energies (see Sec. 3 for details) and the uncertainties result from the energy position of the Gaussian fitting procedure.

$$K + CH_3CH_2OH \rightarrow K^+ + (CH_3CH_2OH^-)^{\#} \rightarrow K^+ + CH_3CH_2O^- + H \quad (1)$$

with (CH_3CH_2O–H) a direct bond breaking, and $(CH_3CH_2OH^-)^{\#}$ formation of a TNI with an excess of internal energy. In the TNI's unimolecular decomposition, autodetachment may successfully compete with formation of a neutral radical and an anion. The branching ratios in Figure 2, which result from the fragment anion yield divided by the total anion yield at a given collision energy, clearly shows that for 8.5 eV collision energy (17.5 eV in the lab frame), OH^- and $CH_3CH_2O^-$ are the solely fragment ions formed, the latter contributing to ~30% of the total anion yield. From the DEA data, the dehydrogenated parent anion is formed via four resonances with increasing intensity as the electron energy is increased at 2.88, 6.35, 7.85 and 9.15 eV, where Ibănescu and co-workers[10] assign the lowest-lying to a shape resonance of σ^*_{OH} antibonding character with a threshold at 2.75 eV. The other high-energy features are due to Feshbach resonances with holes in the n_O and $\bar{n}_O$ oxygen lone pairs, and in the σ_{CH} and σ_{CC} molecular orbitals, respectively.[10,12]

From the data in Table 2, and taking the bond dissociation energy and electron affinity, we obtain $D(CH_3CH_2O–H)–EA(CH_3CH_2O) = 2.78$ eV. Now if we add the potassium ionisation energy of 4.34 eV (see Table 2), such anion ($CH_3CH_2O^-$) formation threshold would be expected at 7.12 eV. Although we have not recorded the dehydrogenated parent anion threshold, a close inspection of the BR in Figure 2 shows that such anion yield below 10 eV tends to decrease as the collision energy decreases, thus suggesting a threshold close to the expected value. Such a reasonable assumption is in accord with methanol dehydrogenated parent anion BR behaviour in the threshold region.[54] The feature in the energy loss spectrum at 7.5 ± 0.1 eV (Figure 3), yields a vertical electron affinity of -3.16 ± 0.10 eV, and is assigned to the σ* shape resonance, although 0.3 eV higher than the DEA experiment.[10] This difference is due to the peak's position uncertainty as well as the estimated energy resolution of the K^+ energy loss data. Note that LUMO + 6 in Fig. S1 calculated at 3.13 eV shows a relevant antibonding character along the O–H bond and in assertion with the assignment in Table 1.

The molecular orbitals in Fig. S1 that can contribute to the energy loss features with vertical excitation energy values at -6.56 ± 0.20, -7.96 ± 0.10 and -9.36 ± 0.10 eV (Table 1), have been assigned to electron transfer from the potassium atom to ethanol's LUMO + 21, LUMO + 33/LUMO + 39 and LUMO + 49/LUMO + 54, respectively, with electron densities exhibiting σ^*_{OH} and σ^*_{CH} antibonding characters. It is worth noting, that such energy values are related with the VUV data of Barbosa et al.'s

Table 2. Gas-phase standard heat of formation ($\Delta_f H_g^\circ$) and electron affinities relevant in dissociative electron attachment to ethanol, taken from Ref.[64] (see text for details).

Compound	$\Delta_f H_g^\circ$ (0 K)[65] (kJ mol^{-1})	$\Delta_f H_g^\circ$ (298.15 K)[64] (kJ mol^{-1})
C_2H_5OH	-217.31 ± 0.20	-235.04 ± 0.21
CH_3CH_3	-68.38 ± 0.12	-84.02 ± 0.12
CH_3CH_2	131.43 ± 0.20	120.63 ± 0.22
CH_2OH	-10.36 ± 0.28	-16.66 ± 0.28
C_2H_4	60.89 ± 0.11	52.38 ± 0.12
CH_2O	-105.392 ± 0.095	-109.229 ± 0.096
OH	37.279 ± 0.022	37.522 ± 0.025
O	246.844 ± 0.002	249.2290 ± 0.0021
CH_3	149.874 ± 0.050	146.471 ± 0.053
CH_2	428.71 ± 0.11 (singlet) 391.050 ± 0.11 (triplet)	429.13 ± 0.11 (singlet) 391.600 ± 0.096 (triplet)
H	216.034	217.998
CH_2^-	328.16 ± 0.18	328.59 ± 0.18
CH_3^-	141.15	137.71
O^-	105.868	108.3
OH^-	-139.063 ± 0.02	-139.030 ± 0.02
$C_2H_5O^-$	-163.88 ± 0.44	-178.81 ± 0.44
	Electron affinity (eV)	
C_2H_5O	1.7120 ± 0.0040	
OH	1.82767	
O	1.439157 ± 0.000004	
CH_3	0.080 ± 0.030	
CH_2	0.652 ± 0.006	
	Bond dissociation energy (eV)	
C_2H_5O–H	4.487 ± 0.032[31] ($\leq$ 4.497 ± 0.022)[32]	
O–H	4.436[66] (4.622[67], 4.35[68])	
	Ionisation energy (eV)	
K	4.34066 ± 0.00001	

features at 6.809 (3sσ), 7.905 (3pπ) and 9.319/9.400 (4pπ) eV[30] of Rydberg character converging to the different ionisation energies of ethanol.[55] Such character is not evident from the electron densities in Fig. S1, yet we have performed TD-DFT calculations on the different electronic states of ethanol negative ion showing the prevalent Rydberg character above 6.0 eV (see Fig. S2). Thus, $CH_3CH_2O^-$ formation may proceed through an internal conversion from a Rydberg to a valence character MO, where avoided crossings are expected to determine the shape of the potential energy surfaces in the representation of the nuclear dynamics. This is in good agreement with DEA experiments of Ibănescu et al.[11] Note that an identical process related to a prevalent intramolecular mechanism of internal conversion yielding dehydrogenated parent anions has been recently observed in electron transfer to methanol[54] and water[48] molecules.

We get back to the dehydrogenated parent anion BR depicted in Figure 2. Although not discernible in the figure, the lowest lying data points show a tendency for increasing from the expected threshold up to 9.3 eV contributing to 34% of the total anion yield, and decreasing with increasing collision energy up to 60 eV. The most relevant yield change occurs between 9.3 and 14 eV, where the excess energy in the TNI is enough to open up other dissociation channels, *viz.* CH_2^-, CH_3^- and O^- formation (see below), and/or intramolecular redistribution through the available degrees of freedom. Above 60 eV collision energy, the $CH_3CH_2O^-$ yield is not strongly energy dependent showing a modest increasing behaviour and contributing on average to ~25% of the total anion yield. This is possibly due to the collision dynamics, where at such energies, the rather fast collision time (<30 fs) does not allow sufficient time for K^+ formed after electron transfer to interact with the TNI via a relevant Coulomb interaction. In the absence of such process allowing effective energy redistribution within the TNI, the metastable parent anion is mostly formed via the fast and direct vertical access above the neutral ground-state, within the Franck-Condon region, yielding a prominent σ^*_{OH} antibonding character of the upper ionic state. The MOs labelled LUMO + 54 and LUMO + 106, at 9.59 and 11.23 eV also contribute to the loss of a hydrogen from the hydroxyl end, yet as the collision energy is increased, a prominent σ^*_{CH} antibonding character is discernible though contributing to the dehydrogenated parent anion formation (see Fig. S1).

3.2. OH^- Formation

Electron transfer in K–CH_3CH_2OH collisions yields OH^- (see BR in Figure 2) as the prevalent fragment anion according to reaction (2):

$$K + CH_3CH_2OH \rightarrow K^+ + (CH_3CH_2OH^-)^{\#} \rightarrow K^+ + OH^- + CH_3CH_2 \quad (2)$$

with (CH_3CH_2–OH) a single bond excision and the extra charge sitting on the hydroxyl radical. The electron affinities of OH and CH_3CH_2O (see Table 2) are almost the same, so one would expect a strong competition between each fragment anions' formation. However, this is not the case across the entire collision energy range investigated but only at higher energies (>130 eV). The hydroxyl anion BR (Figure 2) shows a tendency for increasing from the expected threshold to its maximum at ~9 eV, with also a strong energy dependence up to E_{CM} ~20 eV (accounting for ~45% of the total anion yield), where the fragmentation channels for O^-, CH_3^- and CH_2^- are open. Then, we note an enhancement up to 40 eV and beyond it the yield decreases as the collision energy is increased. Since the collision energy is high enough, thus less efficient stabilization effect of K^+ in the vicinity of the TNI, this may mean that the collision induced fragmentation is dictated by the electron affinity of the radicals resulting in a relevant competition with $CH_3CH_2O^-$ formation. From the values in Table 2, the enthalpy of reaction is $\Delta H_R = 2.79$ eV and adding the potassium atom ionisation energy of 4.34 eV, the threshold of (2) is expected at 7.13 ± 0.10 eV (7.12 ± 0.10 eV for reaction (1)). The electron density for

the neutral molecule in Fig. S1 shows that LUMO + 33 (7.99 eV) has a relevant C–OH antibonding character, whereas LUMO + 37 (8.41 eV) and LUMO + 39 (8.65 eV) have a delocalized shape over –OH. However, at higher energy, LUMO + 54 (9.59 eV) renders special O–H /C–H antibonding characters which are much more in favour of $CH_3CH_2O^-$ formation. Within the TNI, the electron densities in Fig. S2 show prevalent C–OH antibonding character with a calculated electron affinity of 8.22 eV (see also Table 1) in assertion of enhanced hydroxyl anion formation. In the low/intermediate collision energy range, such energy dependence on the hydroxyl anion and dehydrogenated parent anion formation may be responsible for the highest yield of the former fragment anion. Such can exclusively be due to the role of the K^+ formed after electron transfer, where a relevant Coulomb interaction may effectively stabilize the TNI, resulting in effective intramolecular processes that may allow the lowest energetic reactions to evolve. This result is in contrast to DEA experiments where the related reaction threshold (2.79 eV) is considerably below the experimental value of 6.5 eV,[13] thus meaning that more than one neutral fragment can be formed.[13] However, OH^- formation can also proceed via reaction (3):

$$K + CH_3CH_2OH \rightarrow K^+ + (CH_3CH_2OH^-)^{\#} \rightarrow K^+ + OH^- + C_2H_4 + H \quad (3)$$

with ethylene (C_2H_4) and a free hydrogen atom (H) being formed. From the established heats of formation in Table 2, the reaction requires 8.02 eV after adding 4.34 eV from the ionisation energy of K. In case of the neutral molecule, LUMO + 39 (8.65 eV) in Fig. S1, and Fig. S2 (the excited state at 8.22 eV) for the TNI, show a reasonable electron density over C_2H_4 while antibonding characters along O–H and C–H bonds may be discernible, thus supporting also OH^- formation.

3.3. O^- Formation

The TOF mass spectra from charge transfer experiments in neutral potassium atom and neutral ethanol molecule collisions show O^- as the third most abundant fragment anion. In the BRs of Figure 2, the oxygen anion threshold is at ~11.7 eV, increasing up to $E_{CM} = 20$ eV and contributing to ~17% of the total anion yield. Above this energy, the yield is constant regardless the increasing energy in the centre-of-mass system. As the collision energy is increased, the MOs contributing to relevant antibonding character along the C–O and O–H bonds ($\sigma^*_{OH}/\sigma^*_{CH}$) are accessed (e.g., LUMO + 33 and LUMO + 39, Fig. S1) with charge delocalization mostly around CH_3CH_2 (e.g., see (LUMO + 54 in Fig. S1). These MOs also contribute to a relevant competition with OH^- formation, in spite of the less pronounced σ^*_{OH} antibonding character. The feature resulting from the Gaussian fitting in the energy loss spectrum of Figure 3 peaking at 15.5 ± 0.1 eV (Table 1), with a threshold at ~11.9 eV, can also be related to O^- formation via a $\sigma^*_{OH}/\sigma^*_{CO}$ antibonding molecular orbitals (LUMO + 103/LUMO + 106 in Table 1). Such agrees with the calculated electronic excited state of the TNI at 11.29 eV (see Fig. S2) where a relevant Rydberg and C–OH antibonding characters are discernible.

Formation of O^- is associated with two bonds being broken and hydrogen transfer to the α-carbon in ethane,[13] so in potassium-ethanol collisions it may proceed through the following reaction:

$$K + CH_3CH_2OH \rightarrow K^+ + (CH_3CH_2OH^-)^{\#} \rightarrow K^+ + O^- + CH_3CH_3 \quad (4)$$

From the standard heat of formation in Table 2, the thermodynamic threshold of the reaction is 6.98 eV, after adding 4.34 eV for the ionisation energy of the potassium atom. This value is well-below the experimental appearance energy of O^-, and the anion velocity map imaging data reveals no appreciable kinetic energy of the fragment anion.[16] Alternatively, the oxygen anion can be formed via reaction (5):

$$K + CH_3CH_2OH \rightarrow K^+ + (CH_3CH_2OH^-)^{\#} \rightarrow K^+ + O^- + C_2H_5 + H \quad (5)$$

with a calculated threshold of 11.29 eV, in good agreement with the anion threshold at 11.7 eV, within the experimental uncertainty. This is supported by the nature of the lowest unoccupied molecular orbitals of the neutral (e.g., MOs higher than LUMO + 103/LUMO + 106) where a relevant $\sigma^*_{OH}/\sigma^*_{CH}$ character yield the loss of an H atom, either from the hydroxyl or the ethane ends, and a reasonable electron density over C_2H_5 (see Fig. S1), while also in agreement with the antibonding character noted for the TNI in Fig. S2. Above threshold, the electronic state spectroscopy of the attained molecular states is dictated by the prevalent nature of such MOs, i.e., direct access to such antibonding σ* orbitals. Yet, the oxygen anion has been reported in DEA experiments with a broad resonance at ~5.7 eV, but mainly produced via the rearrangement reaction with ethane formation.[13] This is in contrast to the present experimental evidence, showing that the electron transfer collision induced dissociation process is operative via H abstraction, with a dehydrogenated parent anion as an intermediate step, followed by O^- formation. The role of the dehydrogenated parent anion formation as a precursor of further bond excision yielding other fragment anions has been reported in our laboratory for some amino acids[56–58] and more complex molecules as thymine/uracil,[42,59–61] halouracils[37] and adenine,[62,63] just to mention a few.

3.4. CH_2^- and CH_3^- Formation

The BRs in Figure 2 show CH_2^- and CH_3^- as the less intense fragment ions contributing together to ≤ 20% of the total anion yield. As the collision energy is increased the yields are insensitive to the energy, although we can observe a modest tendency of CH_3^- to be enhanced above 70 eV. Nonetheless, such yields are not unexpected given that these anions are formed from the breaking of at least one bond, and the electron affinities of neutral CH_3 and CH_2 are considerably low

as compared to other fragments stemming from electron transfer to ethanol. Another interesting aspect pertains to the nature of the MOs, given the rather antibonding character along the C–C, C–O and C–H bonds (σ^*_{CC}, σ^*_{CO}, σ^*_{CH}) as clearly depicted in LUMO + 103 and LUMO + 106 (see Fig. S1). Formation of CH_3^- is associated with a single bond being broken and it may proceed through the following reaction:

$$K + CH_3CH_2OH \rightarrow K^+ + (CH_3CH_2OH^-)^{\#} \rightarrow K^+ + CH_3^- + CH_2OH \quad (6)$$

From the standard heat of formation in Table 2, the reaction's thermodynamic threshold is 7.95 eV, after adding 4.34 eV for the ionisation energy of the potassium atom. This value is well-below the experimental appearance energy of CH_3^-, i.e., 10.72 eV (Figure 2). Alternatively, CH_3^- can be formed via a more complex reaction (7) which can involve the dehydrogenated parent anion ($CH_3CH_2O^- + H$) formation after the collision complex (K^+ $CH_3CH_2OH^-$) that may further dissociate in:

$$K + CH_3CH_2OH \rightarrow K^+ + (CH_3CH_2OH^-)^{\#} \rightarrow K^+ + CH_3^- + CH_2O + H \quad (7)$$

with a calculated threshold of 11.39 eV (Table 2). An energy difference of ~0.7 eV from the experimental value is noted for such reaction, yet momentum conservation of the dissociating partners may impact the lighter fragment kinetic energy, thus shifting the energy to a higher value. Although a kinetic energy release distribution (KERD) was not recorded, we can rely on the information obtained recently from methanol[54] and water.[48] In these molecules, KERDs for the hydrogen anion were obtained, revealing the role of statistical and direct dissociation in the collision process, where the excess energy was either converted into the available degrees of freedom ($\approx$0.5 eV)[48,54] or being channelled into translational energy of fragments formed (>1.5 eV).[48,54] This is in assertion to Orzol and co-workers[13] DEA experiments in ethanol for the dehydrogenated parent anion formation at the 8.2 eV resonance. As noted, a considerable amount of excess energy on the negative ion is distributed through the available degrees of freedom, while $CH_3CH_2O^-$ carries along more than 5 eV excess energy, yielding the loss of the electron and dissociation.[13]

Following a similar description from CH_3^-, formation of CH_2^- can proceed according to the reactions:

$$K + CH_3CH_2OH \rightarrow K^+ + (CH_3CH_2OH^-)^{\#} \rightarrow K^+ + CH_2^- + CH_3 + OH \quad (8)$$

$$K + CH_3CH_2OH \rightarrow K^+ + (CH_3CH_2OH^-)^{\#} \rightarrow K^+ + CH_2^- + CH_2OH + H \quad (9)$$

with enthalpies of reaction ΔH_r (see Table 2) of 9.45 and 7.79 eV. Now, adding the potassium ionisation energy of 4.34 eV, the expected thresholds are at 13.79 and 12.13 eV. The BR in Figure 2 shows that CH_2^- is formed at a threshold of 13.64 eV, so the contribution of the KERD in reaction (9) may account for the difference of ~1.5 eV, though bringing the expected threshold close to the experimental value. As noted for CH_3^- formation, electron promotion to higher-lying unoccupied molecular orbitals σ^*_{CC}, σ^*_{CO} and σ^*_{CH} antibonding characters may result in CH_2^- formation.

3.5. Energy Loss Spectrum of C_2H_5OH

The K^+ energy loss spectrum data has been smoothed and fitted with Gaussian functions to decompose the energy loss spectrum, with vertical electron affinities and tentative assignment of the main MOs in Table 1. The decomposition procedure was performed on the information obtained from the second derivative of the energy loss spectrum, also considering the energy position of the shape and Feshbach resonances from DEA experiments[10–15] while accounting the width of the Gaussian fittings with the related energy resolution of the charge transfer experiment. The energy loss features above 15 eV have been assigned based on the support from the *ab initio* calculations from the nature of the most relevant molecular orbitals (MOs) involved in the electron transfer process (see Fig. S2). Note that excited molecular states of ethanol with vertical electron affinities of -11.16 ± 0.10, -13.06 ± 0.10, -14.66 ± 0.10 and -16.06 ± 0.10 eV can be associated with features converging to different ionisation limits,[55] i.e., promotion of an electron from $\bar{n}_O/\sigma_{CO}$, n_O/σ_{CC} and $\bar{n}_O/\sigma_{CC}$ MOs to higher orbitals of increasing Rydberg character, mainly *n*p and *n*d (Table 1 and Fig. S2). We have performed calculations at the TD-DFT/ωB97xD/gen level of theory for the lowest-lying electronic states of C_2H_5OH temporary negative ion. Of relevance the nature of the most representative molecular orbitals where a significant electron density delocalization is noted outside the molecular plane with $\sigma^*_{CC}/\sigma^*_{CO}/\sigma^*_{CH}$ antibonding characters (see Fig. S2). Given the considerable large number of molecular states at such high energies, unambiguous assignments of the different Rydberg series are difficult to perform and these have been listed in Table 1 either as $(n+1)$ or as an alternative $(n+2)$.

Ethanol's energy loss spectrum in Figure 3 shows also weak features above 20 eV, with their vertical excitation energies in Table 1. The calculations for C_2H_5OH temporary negative ion lowest lying electronic states predict features at 17.54/18.18, 19.78, 22.48 and 25.89 eV (see Fig. S2). From the shape of the molecular orbitals, although a Rydberg character may be envisaged, for the lowest feature, the majority exhibit strong antibonding character along C–C, C–H and C–O bonds, however, no further tentative assignment has been made for these features. As reported in previous occasions for CH_3OH[54] and H_2O/D_2O,[48] the calculations performed provide information on electronically excited states, accounting only for a single occupied MO being replaced by a non-occupied (virtual) MO, so the role of doubly excited states is not considered. However, we are neither aware of any electron energy loss spectrum in coincidence with Lyman-α photons detection in the inner valence range, nor any cross-sections for Balmer-α fluorescence in the photoexcitation of ethanol above 17 eV, that may provide

relevant information as to the role of singly excited MO states and doubly excited states. This information would be very helpful to assess the role of the strong competition between superexcited states and bond breaking into neutral fragments (and even dipolar dissociation), which was pivotal to assign H_2O/D_2O features above 17 eV in the energy loss spectra of such molecules.[48] Finally, with the lack of further information on the underlying processes governing singly and doubly excited states of ethanol, we hope that the current data may trigger the need to perform complementary experiments and theoretical calculations on the potential energy surfaces and resonance widths of such states.

4. Conclusions

The current electron transfer experiments in collisions of neutral potassium atoms with neutral ethanol molecules have been comprehensively investigated in the laboratory energy range from 17.5 to 350 eV (8.5–170.4 eV in the centre-of-mass frame). Time-of-flight mass spectra in such wide collision energy range have allowed to assign the different fragment anions to OH^-, $C_2H_5O^-$, O^-, CH_3^- and CH_2^-, with no evidence of parent anion formation. The main anion across the entire collision energy range investigated is due to OH^- formation, in strong contrast to dissociative electron attachment experiments where O^- prevails, and together with the dehydrogenated parent anion account for more than 70% of the total anion yield. The branching ratios show a relevant dependence in the low/intermediate collision energies with reaction thresholds showing the relevance of the excess energy in the TNI being channelled either into the different available degrees of freedom or as kinetic energy of the lighter fragments formed. The formation of different fragment anions has been discussed on the basis of the electronic structure mostly supported by quantum chemical calculations. Additional information on the electronic state spectroscopy of CH_3CH_2OH was discussed from the experimental evidence of K^+ energy loss spectrum features. A close comparison with former experimental and theoretical data in the literature, confirms the nature of the lowest-lying electronic states assigned mainly to σ^*_{OH}, σ^*_{CH} and σ^*_{CH} antibonding character, rendering special relevance to the role of the different shape and core-excited Feshbach resonances participating in the electron transfer process. Energy loss features above 11 eV have been assigned to electronic excitations within the TNI to Rydberg orbitals with the aid of quantum chemical calculations. At higher energies ($>$ 20 eV) no attempt was made yet we do not discard the possible role of doubly excited states, which certainly require further investigation about the nature of such transitions.

5. Supplementary Information

The supporting information provides the results of theoretical calculations for the shape of a selection of $K + C_2H_5OH$ Lowest Unoccupied Molecular Orbitals and C_2H_5OH temporary negative ion (TNI) lowest lying electronic states in presence of K.

Author Contributions

A I Lozano and S Kumar: experimental data acquisition; B Kerkeni: software and calculations; P J S Pereira: formal analysis; G García, B Kerkeni and P Limão-Vieira: supervision, writing – review and editing; P Limão-Vieira: funding, resources and supervision.

Acknowledgements

SK acknowledges the Portuguese National Funding Agency (FCT) through PD/BD/142831/2018 and COVID/BD/152673/2022, and together with AIL and PLV the research grant CEFITEC UIDP/00068/2020, DOI: 10.54499/UIDP/00068/2020. This work was also supported by Radiation Biology and Biophysics Doctoral Training Programme (RaBBiT, PD/00193/2012); UCIBIO (UIDB/04378/2020). The computations were enabled by resources provided by the Swedish National Infrastructure for Computing (SNIC) at Chalmers Centre for Computational Science and Engineering (C3SE) and partially funded by the Swedish Research Council through grant agreement no. 2020-05293. GG acknowledges partial financial support from the Spanish Ministerio de Ciencia e Innovación (Project No. PID2019-104727RB–C21). The work is part of COST Action CA18212 - Molecular Dynamics in the GAS phase (MD-GAS).

Conflict of Interests

There are no conflicts to disclose.

Data Availability Statement

The data that support the findings of this study are available from the corresponding author upon reasonable request.

Keywords: Charge transfer · Mass spectrometry

[1] A. Bergantini, P. Maksyutenko, R. I. Kaiser, *Astrophys. J.* **2017**, *841*, 96.
[2] S. B. Charnley, M. E. Kress, A. G. G. M. Tielens, T. J. Millar, *Astrophys. J.* **1995**, *448*, 232–239.
[3] W. V. Kirstine, I. E. Galbally, *Atmos. Chem. Phys.* **2012**, *12*, 545–555. https://doi.org/10.5194/acp-12-545-2012.
[4] T. Kasper, P. Oßwald, U. Struckmeier, K. Kohse-Höinghaus, C. A. Taatjes, J. Wang, T. A. Cool, M. E. Law, A. Morel, P. R. Westmoreland, *Combust. Flame* **2009**, *156*, 1181–1201. https://doi.org/10.1016/j.combustflame.2009.01.023.
[5] H. L. MacLean, L. B. Lave, *Prog. Energy Combust. Sci.* **2003**, *29*, 1–69. https://doi.org/10.1016/S0360-1285(02)00032-1.
[6] V. Naik, A. M. Fiore, L. W. Horowitz, H. B. Singh, C. Wiedinmyer, A. Guenther, J. A. De Gouw, D. B. Millet, P. D. Goldan, W. C. Kuster, *Atmos. Chem. Phys.* **2010**, *10*, 5361–5370. https://doi.org/10.5194/acp-10-5361-2010.

[7] K. L. Nixon, W. A. D. Pires, R. F. C. Neves, H. V. Duque, D. B. Jones, M. J. Brunger, M. C. A. Lopes, *Int. J. Mass Spectrom.* **2016**, *404*, 48–59.
[8] M. J. Brunger, *Int. Rev. Phys. Chem.* **2017**, *36*, 333–376.
[9] M. C. A. Lopes, W. A. D. Pires, K. L. Nixon, R. A. A. Amorim, D. G. M. da Silva, A. C. P. Fernandes, S. Ghosh, D. B. Jones, L. Campbell, R. F. C. Neves, *Eur. Phys. J. D* **2020**, *74*, 88.
[10] B. C. Iba˘nescu, O. May, A. Monney, M. Allan, *Phys. Chem. Chem. Phys.* **2007**, *9*, 3163–3173. https://doi.org/10.1039/b704656a.
[11] B. C. Iba˘nescu, M. Allan, *Phys. Chem. Chem. Phys.* **2008**, *10*, 5232–5237. https://doi.org/10.1039/b806578k.
[12] B. C. Iba˘nescu, M. Allan, *Phys. Chem. Chem. Phys.* **2009**, *11*, 7640–7648. https://doi.org/10.1039/b904945b.
[13] M. Orzol, I. Martin, J. Kocisek, I. Dabkowska, J. Langer, E. Illenberger, *Phys. Chem. Chem. Phys.* **2007**, *9*, 3424–3431. https://doi.org/10.1039/b701543g.
[14] V. S. Prabhudesai, A. H. Kelkar, D. Nandi, E. Krishnakumar, *Phys. Rev. Lett.* **2005**, *95*, 143202. https://doi.org/10.1103/PhysRevLett.95.143202.
[15] V. S. Prabhudesai, D. Nandi, A. H. Kelkar, E. Krishnakumar, *J. Chem. Phys.* **2008**, *128*, 154309.
[16] X. D. Wang, C. J. Xuan, W. L. Feng, S. X. Tian, *J. Chem. Phys.* **2015**, *142*, 064316. https://doi.org/10.1063/1.4907940.
[17] D. Almeida, R. Antunes, G. Martins, G. Garcia, R. W. McCullough, S. Eden, P. Limão-Vieira, *Int. J. Mass Spectrom.* **2012**, *311*, 7–16.
[18] M. A. Khakoo, J. Blumer, K. Keane, C. Campbell, H. Silva, M. C. A. Lopes, C. Winstead, V. McKoy, R. F. Da Costa, L. G. Ferreira, *Phys. Rev. A* **2008**, *77*, 042705.
[19] A. G. Falkowski, M. A. P. Lima, F. Kossoski, *J. Chem. Phys. C* **2020**, *152*, 244302. https://doi.org/10.1063/5.0008428.
[20] W.-C. Tam, C. E. Brion, *J. Electron Spectrosc. Relat. Phenom.* **1974**, *3*, 263–279.
[21] R. Feng, C. E. Brion, *Chem. Phys.* **2002**, *282*, 419–427. https://doi.org/10.1016/S0301-0104(02)00722-X.
[22] L. R. Hargreaves, M. A. Khakoo, C. Winstead, V. McKoy, *J Phys B At. Mol. Opt. Phys.* **2016**, *49*, 185201. https://doi.org/10.1088/0953-4075/49/18/185201.
[23] K. Sunanda, A. K. Das, B. N. Rajasekhar, *J. Quant. Spectrosc. Radiat. Transfer* **2019**, *237*, 106609. https://doi.org/10.1016/j.jqsrt.2019.106609.
[24] A. J. Harrison, B. J. Cederholm, M. A. Terwilliger, *J. Chem. Phys.* **1959**, *30*, 355–356.
[25] H. Koizumi, K. Hironaka, K. Shinsaka, S. Arai, H. Nakazawa, A. Kimura, Y. Ito, Y. Zhang, A. Yagishita, K. Ito, *J. Chem. Phys.* **1986**, *85*, 4276–4279.
[26] M. Ogawa, G. R. Cook, *J. Chem. Phys.* **1958**, *28*, 747–748. https://doi.org/10.1063/1.1744253.
[27] J. C. Person, P. P. Nicole, *J. Chem. Phys.* **1971**, *55*, 3390–3397.
[28] D. R. Salahub, C. Sandorfy, *Chem. Phys. Lett.* **1971**, *8*, 71–74.
[29] H. Tsubomura, K. Kimura, K. Kaya, J. Tanaka, S. Nagakura, *B. Chem. Soc. Jpn.* **1964**, *37*, 417–423.
[30] A. S. Barbosa, M. Mendes, N. C. Jones, S. V. Hoffmann, M. H. F. Bettega, M. J. Brunger, P. Limão-Vieira, *J. Quant. Spectrosc. Radiat. Transfer* **2022**, *285*, 108170. https://doi.org/10.1016/j.jqsrt.2022.108170.
[31] K. M. Ervin, V. F. DeTuri, *J. Phys. Chem. A* **2002**, *106*, 9947–9956. https://doi.org/10.1021/jp020594n.
[32] K. Xu, G. Amaral, J. Zhang, *J. Chem. Phys.* **1999**, *111*, 6271–6282. https://doi.org/10.1063/1.479960.
[33] M. Mendes, B. Pamplona, S. Kumar, F. F. da Silva, A. Aguilar, G. García, M. C. Bacchus-Montabonel, P. Limão-Vieira, *Front. Chem.* **2019**, *7*, 1–10.
[34] M. Mendes, G. García, M. C. Bacchus-Montabonel, P. Limão-Vieira, *Int. J. Mol. Sci.* **2019**, *20*, 6170.
[35] M. Mendes, M. Probst, T. Maihom, G. García, P. Limão-Vieira, *J. Phys. Chem. A* **2019**, *123*, 4068–4073.
[36] S. Kumar, T. Kilich, M. Łabuda, G. García, P. Limão-Vieira, *Phys. Chem. Chem. Phys.* **2022**, *24*, 366–374.
[37] F. F. Silva, D. Almeida, R. Antunes, G. Martins, Y. Nunes, S. Eden, G. Garcia, P. Limão-Vieira, *Phys. Chem. Chem. Phys.* **2011**, *13*, 21621–21629. https://doi.org/10.1039/c1cp22644d.
[38] D. Almeida, F. F. Silva, J. Kopyra, G. García, P. Limão-vieira, *Int. J. Mass Spectrom.* **2014**, *366*, 243–247. https://doi.org/10.1016/j.ijms.2014.01.023.
[39] D. Almeida, F. F. Silva, S. Eden, G. García, P. Limão-Vieira, *J. Phys. Chem. A* **2014**, *118*(4), 690–696.
[40] D. Almeida, F. F. da Silva, G. García, P. Limão-Vieira, *J. Chem. Phys.* **2013**, *139*, 114304.
[41] D. Almeida, M.-C. Bacchus-Montabonel, F. F. da Silva, G. García, P. Limão-Vieira, *J. Phys. Chem. A* **2014**, *118*, 6547–6552.
[42] D. Almeida, R. Antunes, G. Martins, S. Eden, F. Ferreira Da Silva, Y. Nunes, G. Garcia, P. Limão-Vieira, *Phys. Chem. Chem. Phys.* **2011**, *13*(34), 15657–15665. https://doi.org/10.1039/c1cp21340 g.
[43] Illenberger, E.; Momigny, J. *Gaseous Molecular Ions. An Introduction to Elementary Processes Induced by Ionization*; H. Baumgärtel, E. U. Franck, W. G., Ed.; Steinkopff, Springer: Darmstadt, 1992.
[44] A. W. Kleyn, A. M. C. Moutinho, *J. Phys. B At. Mol. Opt. Phys.* **2001**, *4075*, R1–R44.
[45] K. Regeta, S. Kumar, T. Cunha, M. Mendes, A. I. Lozano, P. J. S. Pereira, G. García, A. M. C. Moutinho, *J. Phys. Chem. A* **2020**, *124*, 3220–3227.
[46] A. I. Lozano, L. S. Maioli, B. Pamplona, J. Romero, M. Mendes, F. F. da Silva, F. Kossoski, M. Probst, D. Süβ, M. H. F. Bettega, *Phys. Chem. Chem. Phys.* **2020**, *22*, 23837–23846.
[47] S. Kumar, F. Izadi, M. Ončák, P. Limão-Vieira, S. Denifl, *Phys. Chem. Chem. Phys.* **2022**, *24*, 13335–13342.
[48] S. Kumar, M. Hoshino, B. Kerkeni, G. García, P. Limão-Vieira, *J. Phys. Chem. Lett.* **2023**, *14*, 5362–5369.
[49] R. Antunes, D. Almeida, G. Martins, N. J. Mason, G. Garcia, M. J. P. Maneira, Y. Nunes, P. Limão-Vieira, *Phys. Chem. Chem. Phys.* **2010**, *12*, 12513–12519.
[50] Frisch, M. J.; Trucks, G. W.; Schlegel, H. B.; Scuseria, G. E.; Robb, M. A.; Cheeseman, J. R.; Scalmani, G.; Barone, V.; Petersson, G. A.; Nakatsuji, H.; et al. *Gaussian 16, Revision C.01*; Wallingford CT, 2016.
[51] M. Dolg, P. Fulde, W. Küchle, C. Neumann, H. Stoll, *J. Chem. Phys.* **1991**, *94*, 3011–3017. https://doi.org/10.1063/1.459824.
[52] W. Küchle, M. Dolg, H. Stoll, H. Preuss, *Mol. Phys.* **1991**, *74*, 1245–1263.
[53] M. Petersilka, U. Gossmann, E. K. Gross, *Phys. Rev. Lett.* **1996**, *76*, 1212–1215. https://doi.org/10.1103/PhysRevLett.76.1212.
[54] A. I. Lozano, S. Kumar, B. Kerkeni, G. García, P. Limão-Vieira, *J. Phys. Chem. A* **2022**, *126*, 1076–1084.
[55] S. Katsumata, T. Iwai, K. Kimura, *Bull. Chem. Soc. Jpn.* **1973**, *46*, 3391–3395. https://doi.org/10.1246/bcsj.46.3391.
[56] F. F. Silva, M. Lança, D. Almeida, G. García, P. Limão-Vieira, *Eur. Phys. J. D* **2012**, *66*, 78. https://doi.org/10.1140/epjd/e2012-20751-y.
[57] F. F. Silva, J. Rafael, T. Cunha, D. Almeida, P. Limão-Vieira, *Int. J. Mass Spectrom.* **2014**, *365–366*, 238–242. https://doi.org/10.1016/j.ijms.2014.01.003.
[58] G. Meneses, C. Widmann, T. Cunha, A. Gil, F. F. Silva, M. J. Calhorda, P. Limão-Vieira, *Phys. Chem. Chem. Phys.* **2017**, *19*, 1083–1088. https://doi.org/10.1039/c6cp06375f.
[59] D. Almeida, M.-C. Bacchus-Montabonel, F. F. da Silva, G. Garcia, P. Limão-Vieira, *J. Phys. Chem. A* **2014**, *118(33,SI)*, 6547–6552. https://doi.org/10.1021/jp503164a.
[60] F. F. Silva, C. Matias, D. Almeida, G. García, O. Ingólfsson, H. D. Flosadóttir, B. Ómarsson, S. Ptasinska, B. Puschnigg, P. Scheier, *J. Am. Soc. Mass Spectrom.* **2013**, *24*, 1787–1797. https://doi.org/10.1007/s13361-013-0715-9.
[61] D. Almeida, F. F. Silva, G. García, P. Limão-Vieira, *Phys. Rev. Lett.* **2013**, *110*, 023201.
[62] T. Cunha, M. Mendes, F. F. Silva, S. Eden, G. García, P. Limão-Vieira, *J. Chem. Phys.* **2018**, *148*, 021101. https://doi.org/10.1063/1.5018401.
[63] T. Cunha, M. Mendes, F. F. Silva, S. Eden, G. García, M. C. Bacchus-Montabonel, P. Limão-Vieira, *J. Chem. Phys.* **2018**, *148*, 134301.
[64] NIST Chemistry WebBook, 2023. https://webbook.nist.gov/chemistry.
[65] Argonne National Laboratory. Active Thermochemical Data (ATcT) https://atct.anl.gov/.
[66] J. A. Kerr, *Chem. Rev.* **1966**, *66*, 465–500.
[67] C. W. Bauschlicher, S. R. Langhoff, S. P. Walch, *J. Chem. Phys.* **1992**, *96*, 450–454.
[68] Herzberg, G. *Molecular Spectra and Molecular Structure I. Spectra of Diatomic Molecules*, 2nd ed.; Van Nostrand Reinhold Company: New York, 1950.

Manuscript received: March 20, 2024
Revised manuscript received: April 17, 2024
Accepted manuscript online: April 17, 2024
Version of record online: May 22, 2024